<Invited Paper>

Reconstruction of Two-Dimentional Dielectric Object from Its Scattered Fields by Iterative Inversion in Spectral Domain

Jung-Woong Ra

Ⅰ. INTRODUCTION

The shape and material parameters such as the complex permittivities and permeabilities of an object may be reconstructed from the fields scattered by the object. For a small and low contrasted object, the Born approximation[1],[2] linearizes the relation between the permittivity distribution and the scattered field by approximating the total field inside the penetrable scattering object by its incident field. Diffraction tomography[3] based on this Born approximation relates the permittivity distribution to the Fourier transform of the scattered fields. This method is fast and insensitive to the measurement error.

For high contrasted object where permitivities of the object are much different from the host medium, the moment method inversion[4],[5] may be used to discretize the object into small cells much smaller than the wavelength, such that the fields in each cell may be assumed constant, and then to obtain the polarization current in each cell from the scattered fields. The total field inside the object is obtained from the polarization currents, and the distribution of the permittivity is then obtained by taking the ratio of the polarization current and the total field in each cell. This moment method inversion, however, is shown to suffer from the "illposedness"[6],[7] in a sense that a small error in the scattered fields causes a large error in the polarization currents. The cause of this illposedness may be identified as the exponentially decaying behavior of the evanescent modes, which makes the small error in the evanescent modes of the scattered fields grow exponentially in the back propagating process of the inversion[8],[9].

By selecting only the propagating modes excluding the evanescent modes in the spectrum of the measured scattered fields, the illposedness is regularized without the extra regularization terms of Tikhonov[7] nor the use of the pseudo-inversion, which needs much more measured data points than needed in the moment method inversion[11],[12]. If the total number of cells discretizing the object, N is smaller than the number of the propagating modes of the scattered fields, the errors in the scattered fields do not cause illposedness in the reconstruction of the object by using only the propagating modes[8],[9],[13].

For a large scatterer producing fewer propagating modes of scattered fields P than the number of unknowns, N, the moment method inversion does not give the right reconstruction of the object even with many multiple incident waves, since the polarization currents in each cell vary with different incident waves. Iterative inversion is more effective for this type of reconstruction. One may define a cost functional as the summation of the squared magnitude of the difference between the measured and the calculated scattered fields from the iteratively chosen dielectric profiles. One then minimizes this cost functionals by utilizing the optimizing algorithms such as Levenberg-Marquardt algorithm[14], simulated annealing algorithm[15], and genetic algorithm[16].

The Levenberg-Marquardt (**LM**) algorithm alone is good for reconstructing the low contrasted and small object satisfying the criterion of Born approximation. One needs the stochastic algorithms such as the simulated annealing (**SA**) algorithm or the genetic (**GE**) algorithm to find the global minimum in reconstructing a large and high contrasted object, since there exists many local minima in its cost functional[17],[18]. A hybrid algorithm combining **LM** and **SA**[18] or **GE**[19] is effective in finding the global minimum of the cost functional. Regularization is needed for the iterative inversion and the spectral domain filtering of evanescent modes is effective as in the moment method inversion[18],[19].

Super resolution seems to be obtainable in the reconstruction of the object since the discretization of the object seems to be arbitrary. However, the super resolution requires proper measurement of the scattered fields including evanescent fields which may cause the illposedness in the process of inversion. The scattered fields may be represented as a superposition of plane waves, i.e. the Fourier transformation of the field, say in y-direction, and transformed back, say in z-direction, to the plane of object. The resolution of the reconstruction of the object in the y-direction, say Δy, may then be obtained from

---

Invited Paper

Jung-Woong Ra is with the Department of Electrical Engineering and Computer Science, Korea Advanced Institute of Science & Technology, 373-1, Kusong-Dong, Yusong-Gu, Taejon 305-701, Korea. E-mail : rawoong@ee.kaist.ac.kr

the sampling theorem, $\Delta y \cdot \Delta k = 2\pi$, where Δk is the bandwidth of the spatial frequency of the fields in the object plane in the y-direction, which is the same with that of the measured scattered fields. Measurement of all the propagating modes gives $\Delta k \leq 2k_0$, where k_0 is the wave number of the background medium, and the maximum resolution becomes $\Delta y \geq 1/2\lambda$, where λ is the wavelength. For the super resolution such as $\Delta y \sim 0.1\lambda$, $\Delta k \gg k_0$ is needed and it means the measurement of the evanescent mode fields in addition to the propagating modes.

Non-uniqueness of the inverse solution is often mentioned, by arguing the existence of non-radiating sources. In addition, the existence of the inverse solution is questionable due to the illposedness of the inverse problems. One may filter out the contribution of evanescent modes in the scattered fields at the expense of the resolution of the reconstruction, which regularizes inversion process. One may show that the unique reconstruction of the profile parameters of the penetrable object up to that resolution from the scattered field is possible by the iterative inversion.

Ⅱ. EVANESCENT MODES AND THE ILLPOSEDNESS OF INVERSION

When a time harmonic plane wave having a z-polarized electric field is incident upon a two-dimensional dielectric cylinder having an arbitrary cross section, the total field satisfies the inhomogeneous Helmholtz equation with the source term producing the incident plane wave. If the cross section of the object is given by its distribution of relative permittivities $\varepsilon(\rho)$, where ρ is the two-dimensional cylindrical coordinate vectors, the total fields polarized in the z direction may be represented by the sum of the incident wave and the scattered wave, u^s. The scattered wave is given by an integral[20].

$$u^s(\rho) = k_0^2 \int\int_{S_0} d\rho' [\varepsilon(\rho') - 1] u(\rho) G(\rho, \rho'), \tag{1}$$

where k_0 is the wave number in the background medium, u is the total field inside the dielectric cylinder S_0, ρ, and ρ' are the cylindrical or rectangular coordinate vectors, (ρ, ϕ) and (ρ', ϕ') or (x, y) and (x', y'), respectively, and G is the two-dimensional Green's function in free space. The radiation condition for u^s is satisfied by $G(\rho, \rho')$, and G may be represented either in the configuration or the spectral domain as

$$G(\rho, \rho') = -(j/4) H_0^{(2)}(k_0 |\rho - \rho'|), \tag{2a}$$

$$= -(j/4) \sum_{m=-\infty}^{\infty} J_m(k_0 \rho') H_m^{(2)}(k_0 \rho) e^{jm(\phi - \phi')} \quad \rho > \rho', \tag{2b}$$

$$= \frac{1}{2\pi} \int_{-\infty}^{\infty} d\beta e^{j\beta(y-y')} \frac{e^{-j\sqrt{k_0^2 - \beta^2}|x - x'|}}{2j\sqrt{k_0^2 - \beta^2}}, \tag{2c}$$

where J_m and $H_m^{(2)}$ are the mth order Bessel function and Hankel function of the second kind, respectively, for the time dependence $e^{j\omega t}$.

One may calculate the scattered fields numerically by using the moment method[21],[22] by dividing the cross section S_0 into small cells smaller than $0.2\lambda/\sqrt{\varepsilon}$, where λ is the free space wavelength. The size of the cell is small enough that the polarization current inside each cell is taken as a constant. Substituting (2) into (1), one obtains the integral in (1) for the scattered field by the summation over the total number of cells N, where discretized rectangular cells are replaced by the circular cells[21],[22] of the same area with its radius a, as

$$u^s(\rho) = \sum_{n=1}^{N} [\varepsilon_n(\rho_n) - 1] u_n(\rho_n) I_n(\rho, \rho_n), \tag{3}$$

where ε_n and u_n are the relative permittivity and the total field at $\rho = \rho_n$, respectively,

$$I_n(\rho, \rho_n) = -(j/2)[\pi k_0 a H_1^{(2)}(k_0 a) - 2j], \quad \rho = \rho_n, \tag{4a}$$

$$= -(j/2) \pi k_0 a J_1 H_0^{(2)}(k_0 |\rho = \rho_n|), \quad \rho \neq \rho_n, \tag{4b}$$

from the configuration domain Green's function in (2a). From the spectral domain Green's function in (2b) and (2c) one obtains

$$I_n(\rho, \rho_n) = -(j\pi/2) k_0 a J_1(k_0 a) \sum_{m=-\infty}^{\infty} e^{jm\phi} H_m^{(2)}(k_0 \rho) J_m(k_0 \rho_n) e^{-jm\phi_n}, \quad \rho > \rho', \tag{5}$$

and

$$I_n(\rho, \rho_n) = -\frac{1}{2\pi} \int_{-\infty}^{\infty} d\beta e^{-\beta(y - y_n)} \frac{e^{-j\sqrt{k_0^2 - \beta^2}|x - x_n|}}{2j\sqrt{k_0^2 - \beta^2}} (2k_0 d) \frac{\sin \beta d}{\beta d} \frac{\sin(\sqrt{k_0^2 - \beta^2} d)}{\sqrt{k_0^2 - \beta^2} d}, \tag{6}$$

where Graf's integral theorem[23] of Bessel functions is used in the process of the integral evaluation of (1) and (2b).[13]

To find $\varepsilon(\rho)$ from the integral in (1) is a nonlinear problem. This inversion problem is shifted into finding the polarization current, $(\varepsilon_n - 1)u_n$, in (3) from the measured scattered field $u_s(\rho)$ for the same number of measurement points with the total number of cells, $\rho = \rho_l$, $l = 1, 2, \cdots, N$. This problem becomes linear and its solution is unique if I_n is well defined, where I_n depends upon the geometrical configuration of the discretized cells and measurement points, $|\rho_l - \rho_n| = \rho_{ln}$. Since the cells are discretized much smaller than the wavelength, ρ_{ln} does not change much for the neighboring

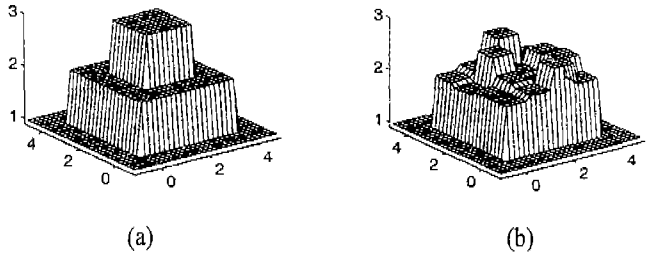

(a) (b)

Fig. 1. "Illposedness" of the moment method inversion in the configuration domain. (a) Orginal profile and (b) reconstructed profile (RMS error = 18.2%) of an inhomogeneous square dielctric cylinder of $0.4\lambda \times 0.4\lambda$ when 0.01% Gaussian noise is added to the scattered fields at $\rho = 0.3\lambda$. Sixteen unknowns with 16 field data are used.

$(n+1)$th cell, and the values of the neighboring column of the matrix $I_n(\rho_{ln})$ in (4) are not much different from $I_n(\rho_{ln+1})$. This makes the inversion of the matrix I_n from (3) and (4) in the configuration domain unstable. If there exists a very small error in the measured scattered field u^s, it causes uncontrollable error in the calculation of $(\varepsilon_n - 1)u_n$, as shown in Fig. 1. This is generally known as the illposedness of Hadamard, and the quadratic constraint[24] in the sense of Tikhonov has been used to regularize the illposedness. Thus, the configuration domain inversion of the polarization current needs an additional regularization term[25] in the inversion of the matrix I_n to compromise the errors in the resultant polarization currents with the stabilization of the inversion process.

This illposedness of the moment method inversion in the configuration domain may be regularized by employing the spectral domain inversion from (3), (5) and (6) and filtering out the higher-order modes of small amplitudes. The normalized modal amplitudes $J_m(k_0\rho_n)$ in (5) for I_n in the spectral domain are plotted in Fig. 2 for a square dielectric cylinder of $1\lambda \times 1\lambda$ and $\varepsilon = 5$. The angular spectral amplitudes of this example without noise in the scattered field decay faster than the exponential decay for modes higher than a critical Mth mode. This may be shown from the asymptotic properties of the mth-order Bessel function[23], since

$$J_m(k_0\rho_n) \sim \frac{1}{\sqrt{2\pi m}}\left(\frac{ek_0\rho_n}{2m}\right)^m, \quad m \gg k_0\rho_n, \tag{7}$$

decreases to the power of small numbers for $2\ m > ek_0\rho_n$, where $e \approx 2.718$ and M is the smallest integer satisfying

$$M \geq ek_0\rho_n/2. \tag{8}$$

When the noise fields of white Gaussian are added to the

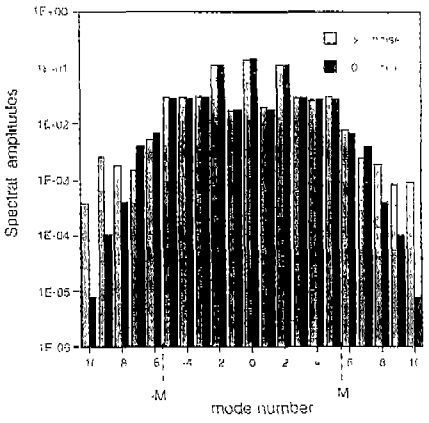

Fig. 2. Computed angular spectrum of the fields scattered by a square dielectric cylinder of $1\lambda \times 1\lambda$ and $\varepsilon = 5$ at $\rho = 5\lambda$ for plane wave incidence from (9).

scattered fields as a measurement error, the noise-added scattered field, $u^s(\rho, \phi)$, may be expanded by its angular modal coefficients,

$$a_m(\rho) = (1/2\pi)\int_0^{2\pi} u^s(\rho, \phi)e^{-jm\phi}\, d\phi. \tag{9}$$

Comparing (9) with (3) and (5), one may identify that the modal coefficients are proportional to the product $H_m^{(2)}(k_0\rho)J_m(k_0\rho_n)$. The modal amplitudes normalized by $H_m^{(2)}(k_0\rho)$ for 5% noise-added scattered field are calculated as in Fig. 2. This shows that the existence of noise affect only the higher-order modes $|m| > 5$, where $M = 5$ is calculated from (8) for the square cylinder of $1\lambda \times 1\lambda$, $\varepsilon = 5$, and $\rho_n = 0.6187\lambda$.

The cause of the illposedness may be explained from the behavior of the product $H_m^{(2)}(k_0\rho)J_m(k_0\rho_n)$ in (5). When a white Gaussian noise distribution is assumed in the scattered fields, the noise power distributed over the modes is uniform. The modal amplitudes of the noiseless scattered field decrease fast for higher modes of $|m| > M$. For the inversion, these scattered fields with noise are transformed into the scattered fields inside the scatterer in which the back propagation via the $H_m^{(2)}(k_0\rho)$ is needed, where $H_m^{(2)}(k_0\rho)$ diverges fast in the near field range, $k_0\rho \ll m$, $m > 0$, as $\sqrt{2/\pi m}(ek_0\rho/2m)^{-m}$. This diverging process amplifies the noise existing in the scattered field in the process of back propagation of the scattered field. This is the same back propagation effect for the plane wave spectrum representation of the Green's function in (6), which amplifies exponentially the noise carried by the evanescent modes of the scattered fields[8]-[10].

It is almost impossible to obtain the original permittivity distribution, since the small numerical errors existing in this

ıoment method inversion are amplified exponentially in the ack propagation process if all the modes of the scattered field re included in the inversion. By filtering out all these igher-order modes and keeping only the lower-order modes of $|m| \le M$, the inversion is stabilized in the presence of noise)r errors) in the scattered fields and any other additional :gularization processes are not needed.

For a realistic inversion the size and the center of the object as to be estimated. Measured scattered fields may be ansformed into a new scattered field with a different origin. he number of effective angular modes of this new scattered eld, neglecting those modes having exponentially small modal mplitudes, becomes minimum when the new origin coincides ith the center of the unknown object. After a few transfor- ıations of the coordinate system with the new origin one may nd the estimated object center and size[26].

The estimated object dimension is discretized into N small ells, as in Fig. 3 and its polarization currents, $(\varepsilon_n - 1)u_n$, ıay be found by inverting (3), where I_n in (5) and a_m in (9) re used with $-M \le m \le M$. Here M is given in (8) with ρ_n epresenting the maximum radius of the estimated object, and ıe total number of the effective modes, P, becomes $2M + 1$. $P > N$, one needs only the N dominant modal coefficients to btain the N polarization currents. Replacing $(\varepsilon_n - 1)u_n$ in (3) y these polarization currents, one obtains $u^s(\rho_n)$ and $u_n(\rho_n) = u^s(\rho_n) + u^i(\rho_n)$, where $u^i(\rho_n)$ is the given incident eld at ρ_n. The complex $(\varepsilon_n - 1)$ is then calculated by ividing $(\varepsilon_n - 1)u_n$ by u_n.

As the maximum radius of the object ρ_m becomes large, the umber of cells N and the critical mode number M are roportional to ρ_m^2 and ρ_m, respectively, and N grows faster ıan M. If $N > P = 2M + 1$ for a large scatterer, one needs dditional data, such as multiple incidences and multi-frequency ources, in order to have the number of data points larger than V. The polarization currents $(\varepsilon_{n-1})u_n$ in (3), however, change)r different incidences and frequencies of the source, so that the umber of unknowns increases. Thus the measurements for dditional sources are of little help, and the moment method ıversion could not give the stable inversion.

Ⅲ. ITERATIVE INVERSION IN THE SPECTRAL DOMAIN

One may utilize the additional data points generated by using ıultiple incidences and frequencies of the source via the erative inversion. The cost function may be defined as the ummation of the squared magnitude of the difference fields etween the measured fields and the fields calculated from the

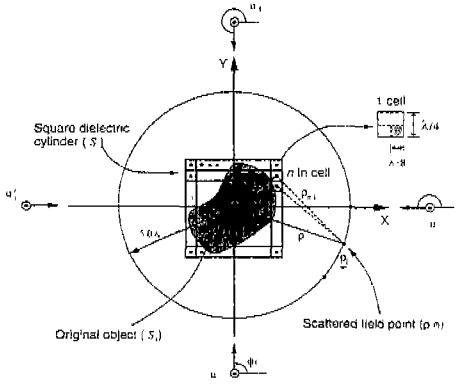

Fig. 3. Plane wave incidence on an arbitrary object which is estimated by the square dielectric cylinder in the inversion.

assumed set of dielectric profiles for the iterations. One then minimizes this cost functional iteratively by updating the distribution of the complex permittivity profile until the original distribution of the complex permittivity is found.

The cost functional f may be defined as

$$f = \frac{1}{2} \sum_{i=1}^{I} \sum_{j=1}^{J} \int_0^{2\pi} d\phi \left| u_M^S(\rho, \phi; \omega_i, \phi_j) - u_c^s(\rho, \phi; \omega_i, \phi_j; \varepsilon_n) \right|^2, \tag{10}$$

where u_M^S and u_c^s are, respectively, the measured and calculated scattered fields from the distribution ε_n, I and J are the total number of different angular frequencies (ω_i), and their incident angles (ϕ_j), respectively, and the squared difference fields are summed over angular angle ϕ in the measurement cylindrical surface of ρ = constant. The measurement error and noise are included in u_M^S. One may convert this functional in the configuration domain into that in the spectral domain by using the Green' s function given in (2b) for the cylindrical measurement.

Substituting (3) and (5) into (10), the integration over ϕ makes the double summation over m in (5) into the single summation over m which may be taken outside of the squared magnitude of F_{mij} as

$$f = \frac{1}{2} \sum_{i=1}^{I} \sum_{j=1}^{J} \sum_{m=-\infty}^{\infty} |F_{mij}|^2, \tag{11}$$

where

$$F_{mij} = H_m^{(2)}(k_0\rho) \left\{ \frac{a_m(\rho; \omega_i, \phi_j)}{H_m^{(2)}(k_0\rho)} - \frac{j\pi k_0 a}{2} J_1(k_0 a) \cdot \sum_{n=1}^{N} (\varepsilon_n - 1) u_n(\omega_i, \phi_j) J_m(k_0 \rho_n) e^{-jm\phi_n} \right\}, \tag{12}$$

a_m given in (9) may be used for the measured fields and the

second term in (12) is obtained from (3) and (5). As shown by equations in (7) and (8), the illposedness occurs when the angular modes m of the measured fields, $|m| \geq M$, one may regularize this inversion by filtering out all these higher-order modes and keeping only the lower order modes of $|m| \leq M$, i.e., the infinite summation over m in (11) is truncated into the finite summation over m from $-M$ to M.

The cost functional defined in (11) and (12) in terms of the angular spectral modes up to $|m| \leq M$ already filters out the noise and does not need any additional measure of regularization.

In order to see the various limitations of the iterative inversion methods, the cost functionals defined in (11) and (12) are calculated as a function of the relative permittivities of the cells ε_n and the object size D. The cost functionals for the fields scattered by a homogeneous circular cylinder of relative permittivity $\varepsilon = 2$ may be calculated as a function of the relative permittivity distribution ε_n, as shown in Figure 4a, by assuming that the measured fields are equal to the exact analytic solution for a plane wave incidence. Three cost functionals in Fig. 4a are for three different sizes of the object diameter D equal to 1 λ, 2 λ, and 4 λ, where λ is the free space wavelength of the source. It shows that only one global minimum occurs at = 2 and many local minima for other values of ε_n depending on D. If D is fixed and e of the object is changed, the calculated cost functionals are shown in Fig. 4b, where the single global minimum occurs for each e equal to 1.5, 3.0, and 5.0 and many other local minima.

In order to find the global minimum of the cost functional defined in (11) and (12) by iterating the kth profile distribution ε_n^k, one may use the Levenberg-Marquardt (**LM**) algorithm where its updating rule minimizing the cost functional is given by[14]

$$\varepsilon(k+1) = \varepsilon(k) - [\,J(k)^T J(k) + \alpha D]^{-1} J(k)^T F \qquad (13)$$

Here $\varepsilon(k)$ is the column vector of ε_n calculated at the k th iterative step, $J(k)$ is the Jacobian matrix describing the increment of the error functional F_{mij} in (11) with respect to ε_n of the nth cell, $\boldsymbol{D}$ is the matrix having only diagonal terms of $J(k)^T J(k)$, $\boldsymbol{F}$ is the column vector having its elements F_{mij}, and the a is the Levenberg-Marquardt parameter regularizing the matrix inversion and improving the convergence rate of the calculation. This algorithm calculates the gradient of the cost function at $\varepsilon(k)$ and gives $\varepsilon(k+1)$ such that the cost functional at $\varepsilon(k+1)$ is decreased until the minimum of the cost functional is found where its gradient becomes zero.

When the initial values of all ε_n are set to 1, the global minimum may be found at $\varepsilon = 2$ from Fig. 4a by the **LM** algorithm for the diameter of the dielectric cylinder $D = 1\ \lambda$. For the other diameters larger than 1 λ the **LM** algorithm finds the values of the nearest minimum from $\varepsilon_n = 1$, that is, $\varepsilon_n \approx 0.7$ for 2 λ and 1.3 for 4 λ. When D is fixed by 2 λ, the initial value of $\varepsilon_n = 1$ makes the **LM** algorithm find the nearest minimum (global) at the original $\varepsilon = 1.5$, as shown in Fig. 4b, but makes it impossible to find the other values of $\varepsilon = 3$ and $\varepsilon = 5$, since the iteration finds the nearest local minimum at the values of $\varepsilon_n \approx 1.3$ and 1.45. It is interesting to observe the range of convergence[25],[27],[28], which turns out to be approximately the same as the criterion of the Born approximation[2],

$$(\sqrt{\varepsilon} - 1) D < (\lambda/2) \qquad (14)$$

The values of e obtained from the Born inversion[29] or the distorted Born iteration[29] may be used as the initial distribution of the **LM** algorithm, but the region of convergence is almost comparable to that in(14).

A source generating a multi-frequency signal makes the depth of the local minima shallower than a single-frequency source but generates more local minima[17]. It does not improve, however, the region of convergence of the **LM** algorithm to the higher-

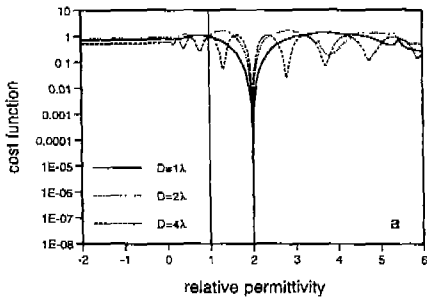

(a)

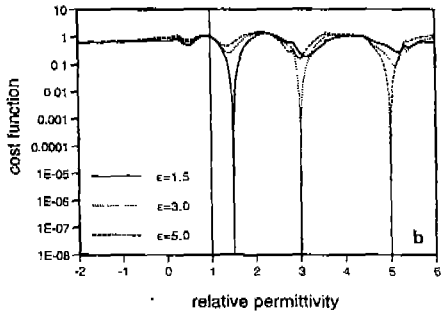

(b)

Fig. 4. Cost functional for a circular dielectric cylinder of (a) $\varepsilon = 2$ and its diameter D as parameter and (b) $D = 1\ \lambda$ and ε as parameter.

contrast objects. One may extend the region of convergence by using the initial distribution obtained from the low-frequency moment method inversion and may obtain the higher-frequency iterative result by using the steepest-descent method[30].

In order to find the profile distribution of the given object scatterer, one needs the algorithm to find the global minimum of the cost functional. **LM** algorithm, however, may be terminated in one of the local minima since it depends upon the initial profiled distribution. The simulated annealing (**SA**) algorithm [15],[18] and the genetic algorithm (**GA**)[16],[19] are used to find the global minimum successfully. A hybrid algorithm combining either **SA** or **GA** with **LM** algorithm is used to find the minimum of the cost functional more effectively for the reconstruction of the large and high-contrast penetrable object such as the scattering object of its size, 3λ by 3λ, having relative dielectric constant $\varepsilon_r = 4.0$ when 10% Gaussian noise is assumed in the measured scattered fields[18],[19]. If the **LM** algorithm traps in one of the local minima, this hybrid algorithm switches **LM** to either **SA** or **GA** to find another permittivity distribution corresponding to the lower cost functional and switches to **LM** again to minimize the functional to reach the deeper minimum and repeats the process until the global minimum is found.

Numerical examples of the successful reconstruction obtained by using the hybrid algorithm are shown in Fig. 5 and Fig. 6. An inhomogeneous larger-size object of $1.25\lambda \times 1.25\lambda$ having its relative permittivity distribution of 3, 5, and 7 is reconstructed in Fig. 5 by the **LM** (Figure 5b), **SA** (Fig. 5c), and hybrid algorithm combining **SA** and **LM** (Fig. 5d) algorithm, respectively, where the result of hybrid algorithm in Fig. 5d is almost the perfect recovery of the original shape and profile. The result of the **SA** algorithm in Fig. 5c gives a close approximation, but it needs more iteration to reach the global minimum. Fig. 6 shows the reconstruction of the two-dimensional homogeneous dielectric cylinder of $\varepsilon_r = 4.0$ with its size of $3\lambda \times 3\lambda$. For this reconstruction, 10 % Gaussian noise is added to the measured scattered fields, and the iterative inversion in the angular spectral domain with the hybrid algorithm combining **LM** and **GA** is used. The cost functional in (11) for this reconstruction is calculated by using 27 angular modes ($2M+1$), four different incident plane waves (j), and five different frequencies (I) with 12×12 cells ($N = 144$) of size $0.5\lambda/\sqrt{\varepsilon_r} \times 0.5\lambda/\sqrt{\varepsilon_r}$. In this case, **GA** uses a population size of 140. The root mean-square error of this reconstruction becomes only 7.96%, which is smaller than the 10% Gaussian noise present in the measured scattered fields.

Fig. 7 shows how the cost functional changes with the number of angular spectral modes (Fig. 7a) and the noise present (Fig. 7b). The cost functional is calculated for a circular

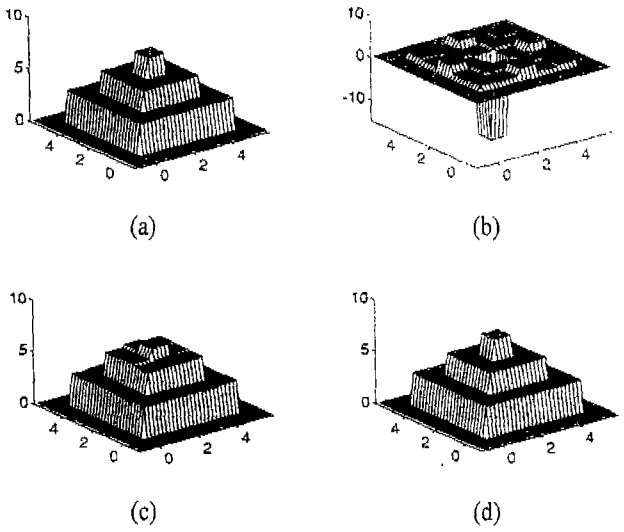

Fig. 5. Reconstructed permittivity of $\varepsilon = 3.5$, and 7 square cylinder with its size $1.25\lambda \times 1.25\lambda$ in (a) original profile and by (b) Levenberg-Marquardt algorithm, (c) simulated annealing algorithm, and (d) hybrid algorithm combining SA and LM for 13 modes with two incident waves.

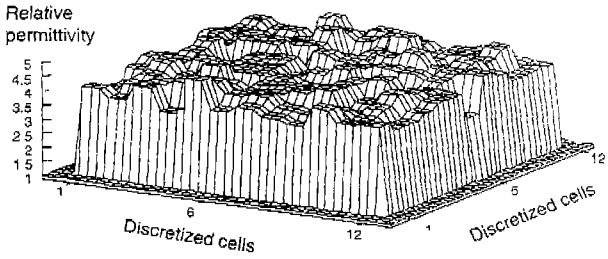

Fig. 6. Reconstruction of the homogeneous dielectric cylinder of its size, $3\lambda \times 3\lambda$, and $\varepsilon_r = 4.0$ in the presence of 10% Gaussian noise in the scattered fields; rms error of the reconstructed permittivity distribution is 7.96%.

dielectric cylinder of diameter 2λ and a relative permittivity of 9. The cost functional with 17 modes, which is the total number of effective modes, shows the distinctive global minimum at $\varepsilon = 9$ and overlaps with that of 31 modes, even in the presence of 5 % Gaussian noise in the scattered fields, as shown Fig. 7b. Very deep local minima indistinguishable from the global minimum exist for the cost functional when a single mode is accounted. In the presence of noise, as shown in Fig. 7b, the local minima of the cost functional are deepened, and the global minimum is shallower and shifted to the slightly different values of relative permittivity.

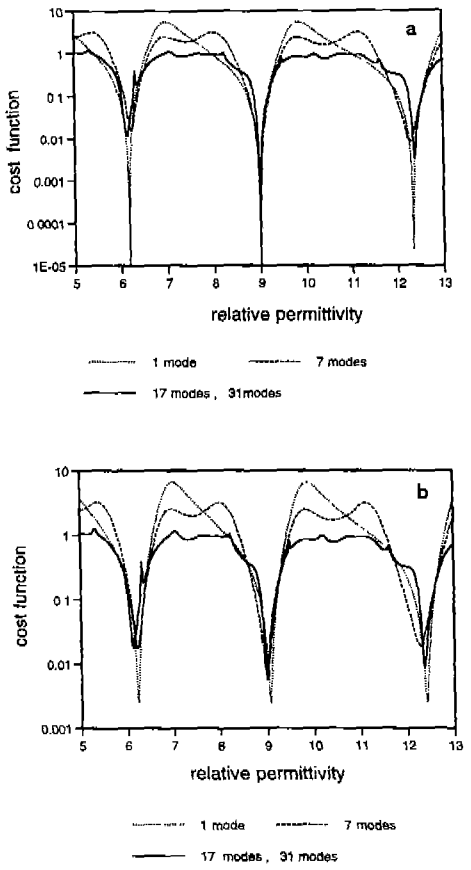

Fig. 7. Cost functional versus relative permittivity as a function of the number of angular spectral modes for a circular dielectric cylinder of $\varepsilon = 9$ and $D = 2\lambda$, (a) without noise and (b) with 5 % Gaussian noise in the scattered fields.

One may speculate that more data points larger than the effective modes do not improve the reconstruction by the iterative minimization even in the presence of noise in the scattered fields. In the presence of noise it is easier to trap in the local minimum, and the reconstructed distribution of permittivities may be deviated slightly.

From the cost functional obtained by an arbitrary dielectric cylinder it is shown that a single global minimum of the cost functional occurs when the total number of the cells of the scatterer N is smaller than KP, where K is the number of multiple views. It is shown numerically that multiple global minima occur in its cost functional if $N > KP$, which prohibits the convergence of the reconstruction to the original profile.

Ⅳ. SAMPLING THEOREM, SUPER RESOLUTION AND UNIQUENESS

Iterative inversion of the two-dimensional thin dielectric object distributed along the y-axis excited by a line source, as shown in Fig. 8, may be used to show the relationship between the resolution of the reconstruction and the sampling of the measured data. The scattered fields in the plane of $x = d$ in Fig. 8 are numerically calculated by the method of moments and used for the measured scattered fields for the iterative inversion. By taking the Fourier transform of the measured scattered fields $U_M^S(d, y)$ in y, one obtains its spatial frequency spectrum $U_M^S(d, \beta)$ as

$$U_M^S(d, \beta) = \int_{-\infty}^{\infty} dy e^{-j\beta y} u_M^S(d, y), \tag{15}$$

where β is the spatial frequency in y-direction. The measured spatial spectrum $U_M^S(d, \beta)$ in the plane of x = d may be transformed into that in the plane of $x = 0$, where the scatteing object is located, via equation in (6) as

$$U_M^S(0, \beta) = U_M^S(d, \beta) e^{j\sqrt{k_0^2 - \beta^2}\, d}, \tag{16a}$$

$$I_m \sqrt{k_0^2 - \beta^2} < 0, \tag{16b}$$

where the imaginary part (I_m) of $\sqrt{k_0^2 - \beta^2}$ is negative for $e^{j\omega t}$ dependence.

The scattered fields may be measured at equally-spaced points in y by the interval of Δy such that

$$N(\Delta y) = L \tag{17}$$

where N and L are the total number and the total length of the measurements in y in the plane of $x = d$. The Fourier transform of the N equally-spaced data of the scattered fields is periodic with period 2π and may be sampled by the same N equally-spaced spatial frequencies for one period by the interval of $\Delta\beta = \frac{2\pi}{L}$ such that its discrete Fourier series reproduces the original discretized scattered fields repeatedly by the period of L. Then one obtains

$$(\Delta y) = \frac{L}{N} = \frac{L}{\left(\frac{B}{\Delta\beta}\right)} = \frac{2\pi}{B}, \tag{18a}$$

$$\Delta\beta = \frac{2\pi}{L}, \tag{18b}$$

where B is the total bandwidth of the spatial frequencies.

Filtering the evanescent modes of the measured scattered fields out and keeping its propagating modes gives $-k_0 \leq \beta \leq k_0$ and $B = k_0$. The relationship in (16) between the measured spectrum in the plane of $x = d$ and back propagated spectrum in the object plane of $x = 0$ is essentially the same with different phase term and gives the resolution (Δy) in the object plane from (18) as

$$(\Delta y) = \frac{2\pi}{B} = \frac{2\pi}{2k_0} = \frac{\lambda}{2}, \tag{19}$$

where λ is the wavelength in free space.

For the super resolution such as $\Delta y \sim 0.1\,\lambda$, the required bandwidth according to the Nyquist sampling theorem in (18) becomes $B = 2\pi / 0.1\,\lambda = 10\,k_0$ which requires the measurements of the evanescent modes in addition to all the propagating modes since $\beta > k_0$. Numerical examples of 24 cell reconstruction shown in Fig. 9 shows that the error of reconstruction increases as the distance of the measurement plane, d in Fig. 8, increases since its bandwidth $B = 5\,k_0$ includes the evanescent modes and its resolution $(\Delta y) = 0.2\,\lambda$ obtained from (19) is used for the reconstruction. Fig. 10 shows that the root mean square error of the reconstruction increases as the resolution of reconstruction increases when the measurement plane is $2\,\lambda$ apart. This shows clearly that the large error occurs for the resolution of reconstruction smaller than $0.5\,\lambda$ which needs the measurement of evanescent modes.

The cost functionals for the fields scattered by a homogeneous circular cylinder shown in Fig. 7 shows that one global minimum exists if the number of modes of the measured scattered field exceeds the total number of unknowns. 5 % Gaussian noise added to the scattered fields does not change the location of the global minimum of the cost functional much, as in Fig. 7, if the higher order modes are filtered out. This implies that the cost functional at the global minimum is bounded if the sufficient number of propagating modes are used as

$$\sum_{i=1}^{I}\sum_{j=1}^{J}\sum_{m=-M}^{M}|F_{ijm}|^2 < \delta, \tag{20}$$

where a small constant d is due to the measurement error. Keeping all the propagating modes means the finite resolution of $0.5\,\lambda$ and the distribution of permittivities of the scattering

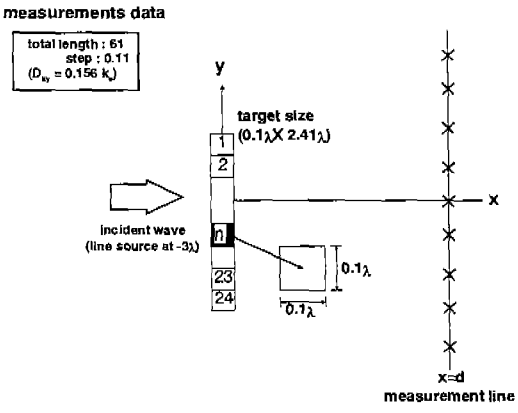

Fig. 8. Iterative inversion from the planar measurement of the scattered fields.

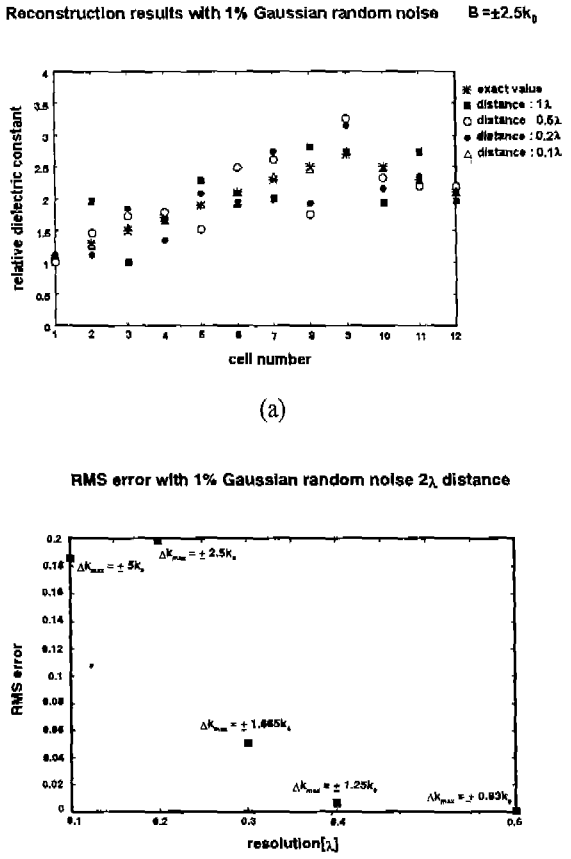

Fig. 9. Iterative reconstruction of dielectric profile of 24 cells in Fig. 8. (a) Bandwidth is fixed by $5k_0$ and the distance of the measurement plane changes from $0.1\,\lambda$ to $1\,\lambda$ when 1% of Gaussian noise is present in the scattered fields. (b) RMS reconstruction error increases as the resolution increases from $0.6\,\lambda$ to $0.1\,\lambda$ when the measurement distance is fixed by $2\,\lambda$ and 1% Gaussian noise is present in the scattered fields.

object discretized by the cells of resolution $0.5\,\lambda$ may be obtained by making F_{mij} in (11) and (12) as

$$\frac{a_m(\rho;\omega_i,\phi_j)}{H_m^{(2)}(k_0\rho)} = \frac{j\pi k_0 a}{2} J_1(k_0 a) \cdot \sum_{n=1}^{N}(\varepsilon_n - 1)\,u_n(\omega_i,\phi_j) J_m(k_0\,\rho_n) e^{-jm\phi_n}, \tag{21}$$

where the total number of equations in (21) becomes $2M + 1 + I + J$, since $2M + 1$, I, and J are the total number of m, i, and j, respectively. This gives a unique reconstruction of N unknowns for $(\varepsilon_n - 1)u_n$, if the total number of modes, $2M + 1 + I + J = N$, since we have N linear independent algebraic

equations for N unknowns.

REFERENCES

[1] A. J. Devaney, "A Computer Simulation Study of Diffraction Tomography", *IEEE Trans. Biomed. Eng.*, vol. 30, pp. 377-386, Jul., 1983.

[2] M. Slaney, A. C. Kak, and L. E. Larsen, "Limitation of Imaging with First-Order Diffraction Tomography", *IEEE Trans. Antennas Propag.*, vol. 14, pp. 460-464, 1966.

[3] A. J. Devany, "Geophysical Diffraction Tomography", *IEEE Trans. Geosci. Remote Sens.*, vol. 22, pp. 3-13, Jan., 1984.

[4] D. K. Ghodgonkar, O. P. Gandhi, and M. J. Hagmann, "Estimation of Complex Permittivities of Three-Dimensional Inhomogeneous Biological Bodies", *IEEE Trans. Microwave Theory Tech.*, vol. 31, pp. 442-446, 1983.

[5] S. A. Johnson, T. H. Yoon, and J. W. Ra, "Inverse Scattering Solutions of the Scalar Helmholtz Wave Equation by a Multiple Source, Moment Methods", *Electron. Lett.*, vol. 19, pp. 130-132, 1983.

[6] J. Hadamard, *Lecture on the Cauchy Problem in Linear Partial Differential Equation,* Yale Univ. Press, New Haven, Conn., 1923.

[7] A. N. Tikhonov and V. Y. Arsenin, *Solutions of Ill-Posed Problems,* Winston, Washington, D. C., 1977.

[8] J. M. Lee, S. Y. Kim, and J. W. Ra, "A Spectral Inverse Technique for Reconstruction of Complex Permittivity Profiles", *Electron. Lett.*, vol. 24, pp. 556-558, 1988.

[9] S. Y. Kim, H. C. Choi, J. M. Lee, and J. W. Ra, "Inverse Scattering Scheme Based on the Moment Method in the Spectral Domain, I, Theory", *Ultrason. Imaging,* vol. 14, pp. 16-28, 1992a.

[10] S. Y. Kim, H. C. Choi, J. M. Lee, and J. W. Ra, "Inverse Scattering Scheme Based on the Moment Method in the Spectral Domain, II, Numerical Simulation", *Ultrason. Imaging,* vol. 14, pp. 29-39, 1992b.

[11] M. M. Ney, A. M.. Smith, and S. S. Stuchly, "A Solution of Electo-Magnetic Imaging Using Psudoinverse Transformation", *IEEE Trans. Medical Imaging,* vol. 3, pp. 155-162, 1984.

[12] S. Caorsi, G. L. Gragnani, and M. Pastorino, "Two-Dimensional Microwave Imaging by a Numerical Inverse Scattering Solution", *IEEE Trans. Microwave Teory Tech.*, vol. 38, pp. 981-989, Aug., 1990.

[13] K. S. Lee and J. W. Ra, "Angular Spectral Inversion for Reconstruction of Complex Permittivity Profiles", *Microwave Opt. Technol. Lett.*, vol. 5, Aug., 1992.

[14] J. E. Jr. Dennis, *Numerical Methods for Unconstrained Optimization and Nonlinear Equations*, Prentice-Hall, Englewood Cliffs, N. J., 1983.

[15] L. Garnero, A. Franchogis, J. P. Hugonju, C. Pichot, and N. Joachimowicz, "Microwave Imaging-Complex Permittivity Reconstruction by Simulated Annealing", *IEEE Trans. Microwave Theory Tech.*, vol. 39, pp. 1801-1809, Nov., 1991.

[16] D. E. Goldberg, *Genetic Algorithms in Search, Optimization and Machine Learning, Addison-Wesley,* Reading, MA, 1989.

[17] C. S. Park, S. K. Park, and J. W. Ra, "Microwave Imaging in Angular Spectral Domain Based on the Improved Newton's Procedure", *Microwave Opt. Technol. Lett.*, vol. 7, pp. 28-31, Jan., 1994.

[18] C. S. Park, S. K. Park, and J. W. Ra, "Moment Method Inversion of Two-Dimensional Complex Permittivity Profiles by Using Effective Modes with Multiple Sources in The Presence of Noise", *Radio Sci.*, vol. 31, pp.1877-1886, Nov.-Dec. 1996.

[19] S. Y. Yang, H. K. Choi, and J. W. Ra, "Reconstruction of a Large and High-Contrast Penetrable Object by Using the Genetic and Lenvenberg-Marquardt Algorthms", *Microwave Opt. Technol. Lett.*, vol. 16, pp17-21, Sep., 1997.

[20] W. C. Chew, *Waves and Fields in Inhomogeneous Media,* Van Nostrand Reinhold, New York, 1990.

[21] J. H. Richmond, "Scattering by a Dielectric Cylinder of Arbitrary Cross Section Shape", *IEEE Trans., Antennas Propag.*, vol. 13, pp. 334-341, May, 1965.

[22] J. H. Richmond, "TE-Wave Scattering by Dielectric Cylinder of Arbitrary Cross-Section Shape", *IEEE Trans, Antennas Propag.*, vol. 14, pp. 460-464, 1966.

[23] M. Abramowitz and I. A. Stegun, (Eds.), *Handbook of Mathematical Functions with Formulas, Graphics, and Mathematical Tables,* Dover, Mineola, N. Y., 1972.

[24] K. Miller, "Least Squares Methods for Ill-Posed Problems with a Prescribed Bound", *SIAM J. Math. Anal.*, vol. 1, pp. 52-74,1970.

[25] N. Joachimowicz, C. Pichot, J. P. Hugonin, "Inverse Scattering: An Iterative Numerical Method for Electromagnetic Imaging", *IEEE Trans. Antennas Propag.*, vol. 39, pp. 1742-1752, Dec., 1991.

[26] S. K. Park, C. S. Park and J. W. Ra, "Iterative Angular-Mode Inversion of a Conducting Cylinder", *Microwave and Opt. Technol. Lett.*, vol. 10, Mar., 1995.

[27] D. T. Borup, S. A. Johnson, W. W. Kim, and M. J. Berggren, "Nonpeturbative Diffraction Tomography via Gauss-Newton Iteration Applied to the Scattering Integral Equation", *Ultrason, Imaging,* vol. 14, pp. 69-85, 1992.

[28] T. Takenaka, "On a Simple Diffraction Tomography Technique based on a Modified Newton-Kantorovich Method", *Microwave Opt. Technol. Lett.*, vol. 5, pp. 94-97,

Feb., 1992.

[29] W. C. Chew and Y. M. Wang, "Reconstruction of Two-Dimensional Permittivity Distribution Using the Distorted Born Iterative Method", *IEEE Trans. Medical Imaging*, vol. 9, pp. 218-246, Feb., 1990.

[30] W. C. Chew and J. H. Lin, "A Frequency-Hopping Approach for Microwave Imaging of Large Inhomogeneous Bodies", *IEEE Antennas Propag. Soc. Int. Symp.*, vol. 3, pp. 1610-1613, 1995.

Jung-Woong Ra

1963 : Seoul National University, Seoul, Korea, B. S. in Electronics Engineering

1967 : Polytechnic Institute of Brooklyn, N. Y., USA, M.S. in Electrophysics

1971 : Polytechnic Institute of Brooklyn, N. Y., USA, Ph. D in Electrophysics

1971~ present : Professor, Department of Electrical Engineering and Computer Science, Korea Advanced Institute of Science and Technology

1992~ present: Editorial Board members, Microwave and Optical Technology Letters, John Wiley & Sons.

1994~ 1995: General Chairman, Asia Pacific Microwave Conference '95

1994~ present: President, URSI(International Union of Radio Science) South Korea

1997: President, Korea Institute of Telematics and Electronics (English name is now changed to Institute of Electronics Engineers of Korea(IEEK))

1996~1998: IEEE MTT-S administrative committee member; Chairman of MTT-S Transnational Committee

1997~1998: General Chairman, ITC CSCC '98

1997~1998: General Chairman, KJJC-AP/EMC/EMT

Research Interests : Microwave Engineering, Forward and Inverse Scattering of Waves, Electromagnetic Geophysical Remote Sensing.